bioRxiv preprint doi: https://doi.org/10.1101/2024.12.19.629259; this version posted December 22, 2024. The copyright holder for this preprint (which was not certified by peer review) is the author/funder, who has granted bioRxiv a license to display the preprint in perpetuity. It is made available under aCC-BY-NC-ND 4.0 International license.

CALIPERS: Cell cycle-aware live imaging for phenotyping experiments and regeneration studies

Moises Di Sante[1,*], Melissa Pezzotti[1], Julius Zimmermann[1], Alessandro Enrico[1], Joran Deschamps[2], Elisa Balmas[3], Silvia Becca[3], Alessandro Reali[1], Alessandro Bertero[3], Florian Jug[2], Francesco S. Pasqualini[1,*]

1. Synthetic Physiology Laboratory, University of Pavia, Italy
2. Human Technopole, Milan, Italy
3. Molecular Biotechnology Center "Guido Tarone", University of Torino, Italy

* Corresponding authors: francesco.pasqualini@unipv.it; moises.disante@unipv.it

Abstract

Measuring cell structure and function along with cell cycle progression in live cell imaging has been challenging because Fluorescence Ubiquitin Cell Cycle Indicators (FUCCI) and most phenotypic sensors both utilize green (GFP) and red (RFP) fluorescence proteins. We introduce CALIPERS, a method for cell cycle-aware live-cell imaging for phenotyping experiments and regeneration studies. CALIPERS uses a custom FUCCI sensor called FUCCIplex that spectrally multiplexes with GFP and RFP-based sensors. To demonstrate the broad range of applications for CALIPERS, we validated it with epithelial and human induced pluripotent stem cell multi-color reporter lines in proliferation, migration, cardiac drug testing, and regenerative medicine studies.

Main text

The convergence of -omics and imaging techniques is powering advanced assessments of cellular phenotypes in basic science[1,2], drug testing[3], and regenerative medicine[4]. Further, reference human induced pluripotent stem cells (hiPSCs) and robust protocols for multilineage differentiation (e.g., cardiac muscle cells, hiPSC-CM) strengthened reproducibility[5] and extended phenotyping efforts to organoids[6,7] and organs-on-chips[8,9]. However, the cell cycle (CC) can confound these studies because gene expression, morphology, and behavior change as cells grow after division (G1 phase), duplicate their DNA (S), grow before subsequent divisions (G2), or divide (M)[10]. This is well addressed in molecular phenotyping, as most -omics efforts are CC-aware thanks to the simultaneous measurement of many CC genes/proteins[11]. However, imaging-based CC-aware phenotyping is challenging. Structural phenotyping of chemically fixed samples can be made CC-aware via specific staining for G1/S/G2/M markers[12]. However, functional phenotyping is only possible through live-cell imaging[13,14], where it is presently difficult to assess the CC together with cell structure and function using standard fluorescence microscopes. In fact, green and red fluorescent proteins (GFP, RFP) power both Fluorescence Ubiquitin Cell Cycle Indicators (FUCCI)[10] and most phenotypic sensors[15].

Here, we introduce a multiplexable FUCCI sensor, FUCCIplex, and demonstrate CC-aware live imaging for phenotyping experiments and regeneration studies (CALIPERS) in human epithelial cells (HaCaT, Fig. 1) and hiPSCs (Fig. 2). To create FUCCIplex, we re-placed GFP and RFP in the fastFUCCI sensor[16] with miRFP670 (iRFP) and mTurquoise2 (CFP). Thus, the nucleus of FUCCIplex cells contains CFP in G1, both CPF and iRFP in the G1-S transition, and only iRFP during the S/G2/M phases (Fig. 1a). To showcase CALIPERS, we co-expressed FUCCIplex in HaCaT cells together with the actin-binding peptide RFP-LifeAct[17] and used live-cell fluorescence imaging over 40 hours to track the time cells spent in each CC phase (Fig. 1b and Supplemental Video 1 and 2). We confirmed that HaCaT cells spent ~40% of their time in G1 and the rest in S/G2/M, in good agreement with CC phase occupancies measured in static images and flow cytometry experiments with FUCCIplex or a DNA marker (Fig. 1c-d and Extended Figure 1). Also, we developed an open-source plug-in that converts CFP and iRFP intensities into a FUCCIphase signal that tracks the CC percent completion and enables CC-aware morphology and motility analyses (Fig. 1e, Supplemental Video 3, and Extended Figure 2).

bioRxiv preprint doi: https://doi.org/10.1101/2024.12.19.629259; this version posted December 22, 2024. The copyright holder for this preprint (which was not certified by peer review) is the author/funder, who has granted bioRxiv a license to display the preprint in perpetuity. It is made available under aCC-BY-NC-ND 4.0 International license.

To enable long-term live imaging with FUCCIplex, we chose CFP to avoid phototoxic UV-shifted species[18]. Since CFP and GFP partially overlap, we developed two approaches to creating four-color reporter lines. For late CC events like mitotic spindle formation[19], we leveraged the lack of bleed-through in S/G2/M. We fused GFP to β-tubulin to enable a smart microscopy routine that maximizes spindle acquisitions and minimizes phototoxicity. We image ten separate cells over 24 hours by switching from 2D widefield fluorescence to 3D confocal imaging when the FUCCIphase signal in each cell reached ~90%. Overall, phototoxicity was comparable with automatically acquiring a volume every six hours, but spindle yield was on par with imaging a volume every hour. Thanks to the reduced phototoxicity, up to five volumes per division could be acquired. (Fig. 1g-h, Extended Figures 3 and 4, and Supplementary Video 5). Alternatively, for a multiplexing strategy that works in all CC phases, we combined FUCCIplex with a faster GFP-based calcium sensor, as calcium transients are orders of magnitude faster than the CC. To demonstrate this approach, we treated HaCaT cells with a GFP-based calcium-sensitive dye, imaged ATP-induced calcium releases, and automatically extracted CC-aware morphological and intensity-based features after removing the static CFP nuclear bleed-through artifact. (Fig. 1f, Supplemental Video 4, and Supplemental Figure 2).

bioRxiv preprint doi: https://doi.org/10.1101/2024.12.19.629259; this version posted December 22, 2024. The copyright holder for this preprint (which was not certified by peer review) is the author/funder, who has granted bioRxiv a license to display the preprint in perpetuity. It is made available under aCC-BY-NC-ND 4.0 International license.

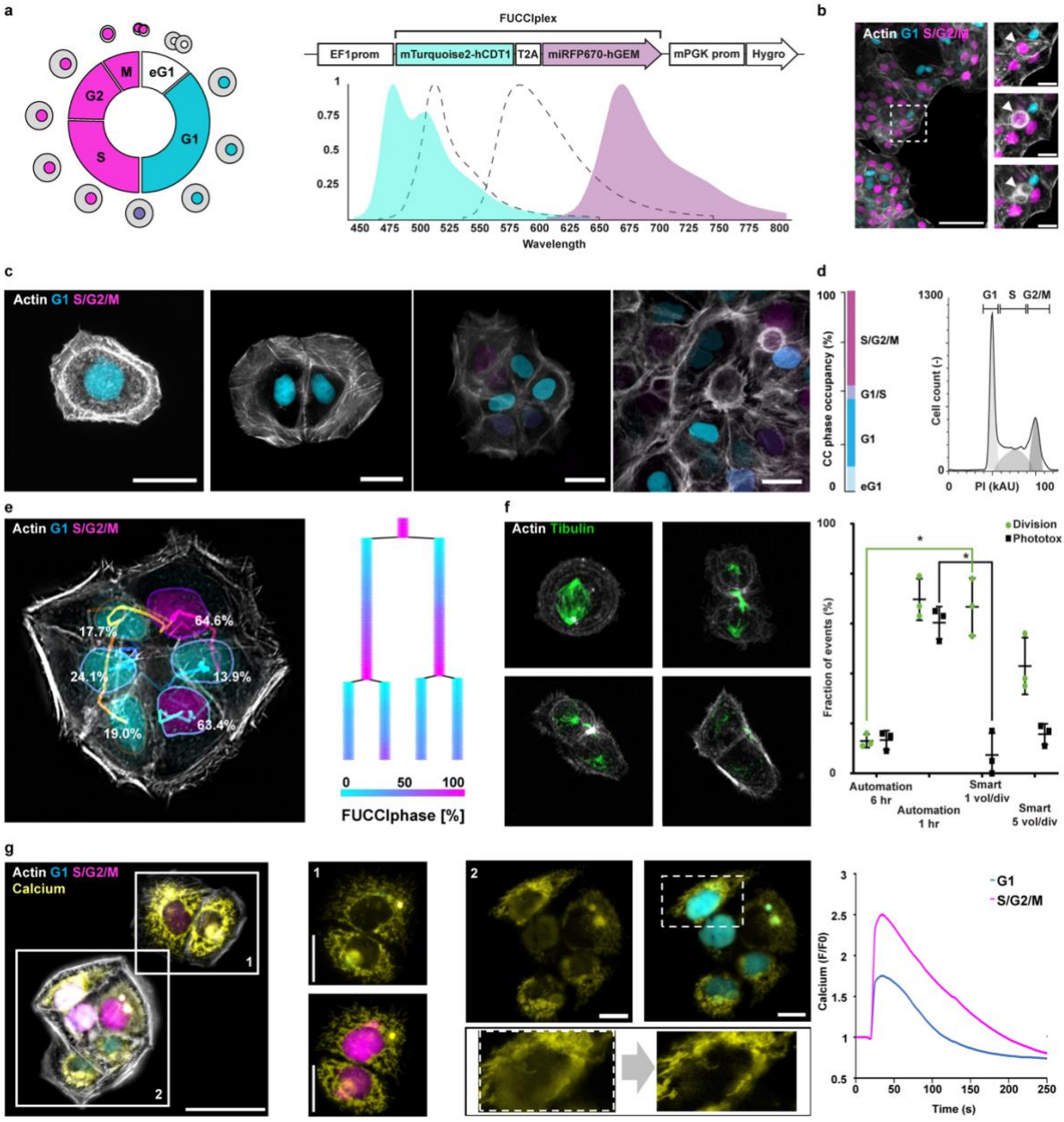


Figure 1: Demonstrating CALIPERS in HaCaT cells. a) FUCCIplex expected readouts at every cell cycle (CC) phase and a representation of the multiplexable emission spectra (GFP and RFP spectra are dashed). **b-c)** Live imaging of HaCaT cells expressing FUCCIplex (cyan/magenta) and RFP-LifeAct (grey). Insets show a cell before and after division. **d)** CC phase occupancy based on flow cytometry of FUCCIplex-expressing HaCaT (left) or WT cells stained with PI (right). **e)** A frame from a live cell imaging video of migrating and proliferating HaCaT cells and a portion of the cell hierarchy. The CC is calculated with an open plugin (FUCCIphase) for every cell and every frame and is used to overlay the CC percentage with the movie. **f)** Representative smart microscopy acquisition of mitotic spindle dynamics in FUCCIplex-LifeAct HaCaT cells with GFP-tagged β-tubulin. Statistical comparison of smart microscopy spindle yield and phototoxicity versus automatic confocal acquisitions every one or six hours. Three independent experiments, results as mean ± SD, $p<0.05$ (*). **g)** Live imaging of HaCaT cells with a calcium-sensitive dye (FLUO-4, yellow), no miRFP670 bleed-through in S/G2/M cells (panel 1), and CFP bleed-through removal in G1 cells (panel 2). Scale bars: 100 µm (a), 15 µm (b), 25 µm (elsewhere).

bioRxiv preprint doi: https://doi.org/10.1101/2024.12.19.629259; this version posted December 22, 2024. The copyright holder for this preprint (which was not certified by peer review) is the author/funder, who has granted bioRxiv a license to display the preprint in perpetuity. It is made available under aCC-BY-NC-ND 4.0 International license.

Having validated CALIPERS with canonical CC events in HaCaT, we deployed it in hiPSCs. To maximize the multiplexing advantage in the field, we used the same WTC-11 reference hiPSCs that originated the dozens of lines pre-tagged with GFP and RFP sensors in the Allen Cell Collection[5]. To further extend our analysis, we focus on the applications of hiPSC-CMs in drug discovery and regenerative medicine, where success depends on CC-aware phenotyping during noncanonical CC events: CC exits (G0 phase) and re-entries via proliferation, multinucleation, or endoreplication[20] (Fig. 2a). Practically, we first engineered a line expressing RFP-LifeAct and GCaMP6f to enable live cell imaging of two key hiPSC-CM phenotype indicators: myofibril organization and calcium transients (Extended Fig. 5)[13,14]. Then, we screened several lentiviral vectors to express FUCCIplex in hiPSCs and hiPSC-CMs using constitutive and cardiac-specific promoters. Our results confirmed that FUCCIplex can be expressed in both cell types and that most hiPSC-CMs had G0, cyan nuclei (Extended Figure 6). We noticed that under the EF1α promoter, FUCCIplex was expressed in hiPSCs, germ layers, and 3D embryoid bodies but not in hiPSC-CMs, so we used the free far red channel to further multiplex the cell microtubule dynamics[21] (Fig. 2b-c, Extended Figure 7a-c, and Supplementary Video 7).

We reasoned that a hiPSC line in which FUCCIplex turns OFF in hPSC-CMs can be useful in personalized cardio-oncology[22,23], where one starts with the same patient-specific hiPSCs and seeks to determine a compound's killing efficiency in cycling tumor cells and its potential toxicity in non-cycling cardiac muscle. To demonstrate this approach, we differentiated 3D cardioids[6] from an hiPSC clone before performing single-cell RNA sequencing to confirm the presence of multiple cardiac cell types and the reduced expression of FUCCIplex in transcriptionally more mature hiPSC-CMs (Fig. 2d-e, Extended Figure 7d-f and 8, and Supplementary Video 8). Then, we administered the microtubule-targeting cancer drug nocodazole to cycling and non-cycling hiPSC-derived cells. In cycling cells, we saw M phase accumulation, abnormal CC re-entry, and cell death, as expected[24] (Extended Figure 7g and Supplemental Video 9). In hPSC-CMs, we saw reversible microtubule depolymerization but sustained calcium cycling alterations (Fig. 2f and Supplemental Video 10-12), suggesting a role for calcium micro-domains[25] in cardio-oncology[22,23].

Finally, in cardiac regenerative medicine, there is a need to screen for therapies that induce CC re-entry[26,27] while integrating mature structure and function at the regeneration site[4,28]. To this end, we created a hiPSC stably expressing FUCCIplex by genome-editing it under the control of the constitutive CAG promoter in the human Rosa26 locus[29] (Extended Figure 9). In the resulting four-color hiPSC reporter line, terminally differentiated hPSC-CMs expressed nuclear CFP, typical of G0 cells[30]. However, based on far-red fluorescence, we could identify rare hPSC-CMs re-entering the CC and perform CC-aware structural and functional phenotyping before/after proliferation (Fig 2g and Supplementary Video 13-14), multinucleation (Fig 2h and Supplementary Video 15-16), and endoreplication (Fig 2i and Supplementary Video 17-18) events[20,30]. Notably, these analyses could be extended in content (Extended Figure 10a and Supplementary Video 19) and throughput (Extended Figure 10b and Supplementary Video 20).

In conclusion, we introduced CALIPERS, a method for CC-aware live imaging for phenotyping experiments and regeneration studies that only uses standard microscopes and filter sets. We validated CALIPERS in live-cell imaging experiments lasting 12-40 hours, often combining fast functional acquisition with slower structural changes. Furthermore, we propose a new reference hiPSC line where FUCCIplex is paired with actin and calcium sensors relevant across indications. We also validated multiple reagents and strategies to genetically encode FUCCIplex, thus enabling CALIPERS in cell lines and hiPSCs with arbitrary GFP/RFP-based sensors[15], including the widely adopted cells in the Allen Cell Collection[5]. Finally, we developed freely available software tools, like FUCCIphase and FUCCIsmart, that can be adopted with most FUCCI types[10,16]. Overall, we are confident that CALIPERS will extend to live cell imaging the same advantages that CC-awareness offers -omics-based disciplines.

Materials and Methods. An extensive materials and methods section is provided in the Supplementary Information file together with links to GitHub repositories and scRNAseq datasets and analyses.

bioRxiv preprint doi: https://doi.org/10.1101/2024.12.19.629259; this version posted December 22, 2024. The copyright holder for this preprint (which was not certified by peer review) is the author/funder, who has granted bioRxiv a license to display the preprint in perpetuity. It is made available under aCC-BY-NC-ND 4.0 International license.

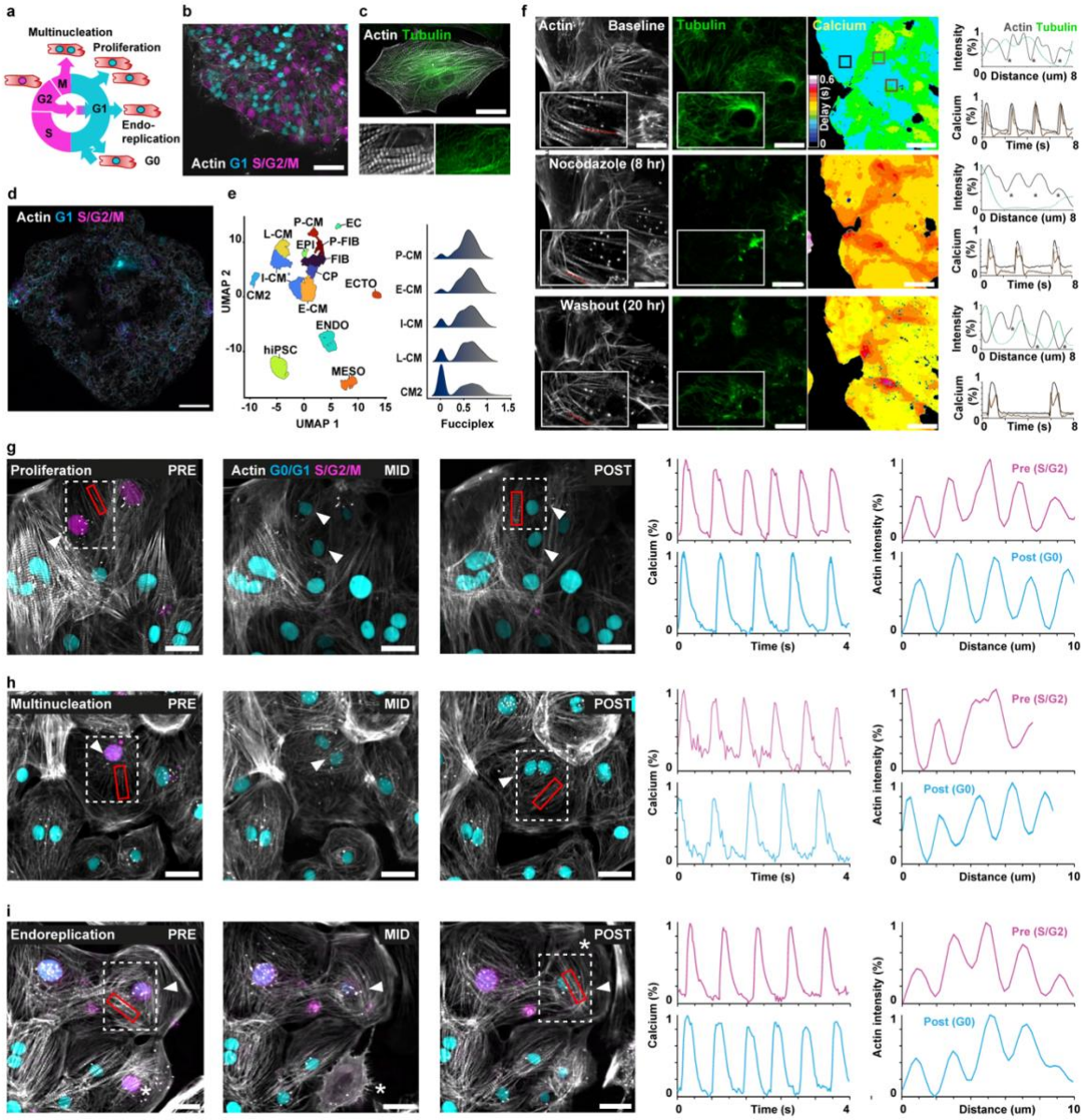


Figure 2: Deploying CALIPERS in hiPSCs. a) FUCCIplex expected readouts of non-canonical CC events in cardiomyocytes. **b)** hiPSC colony expressing LifeAct (grey) and FUCCIplex (cyan/magenta) from the EF1α promoter. **c)** Frame from an EF1α-FUCCIplex hiPSC-CM showing sarcomeres and microtubules (insets) thanks to a microtubule dye (green) imaged in the far-red channel after FUCCIplex turned OFF in hiPSC-CMs. **d)** Cardiac organoid formation from EF1a-FUCCIplex hiPSCs. **e)** Single-cell RNAseq of EF1α-FUCCIplex hiPSCs, tri-lineage differentiated endoderm (ENDO), mesoderm (MESO), ectoderm (ECTO), and cardioid-differentiated endothelial cells (EC), epicardial cells (EPI) proliferating fibroblasts (P-FIB), fibroblasts (FIB), cardiac progenitors (CP), early (E-CM), proliferating (P-CM), intermediate (I-CM), late (L-CM), and conductive cardiomyocytes (CM2),. **f)** Structural (actin: grey, tubulin: green) and functional (calcium: chronomaps) analysis of nocodazole effect on EF1α-FUCCIplex hiPSC-CMs. **g-i)** CC-aware phenotyping of hROSA26-CAG-FUCCIplex hiPSC-CMs that constitutively express FUCCIplex showing hiPSC-CMs re-entering the CC (miRFP-expressing nuclei) during proliferation (**g**), multinucleation (**h**), or endoreplication (**i**). Dashed squares and arrowheads indicate a cell before and after division in all conditions; the asterisk indicates an additional proliferation event in the endoreplication panels. Scale bars: 100 µm (b, d), 25 µm (elsewhere).

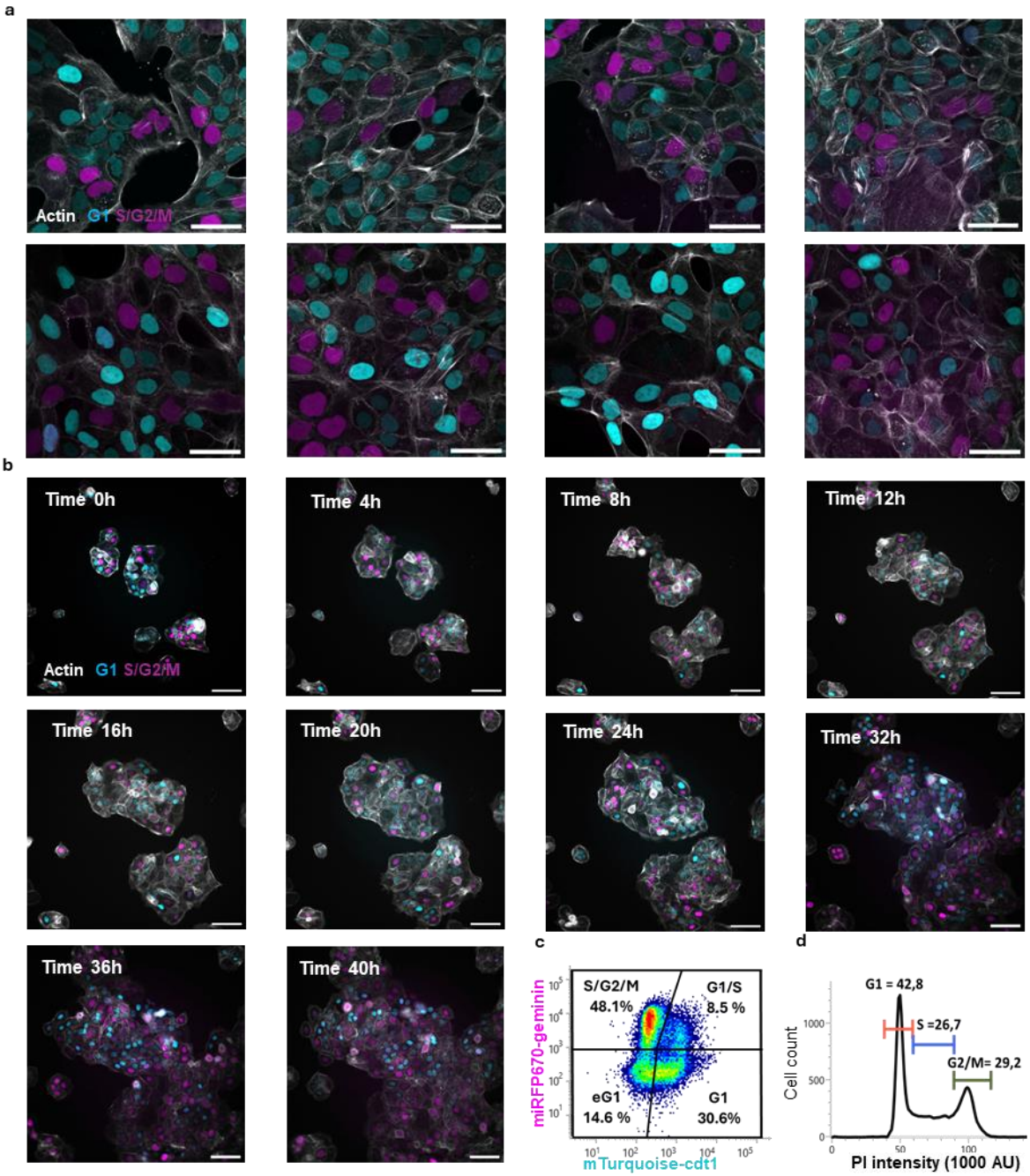
bioRxiv preprint doi: https://doi.org/10.1101/2024.12.19.629259; this version posted December 22, 2024. The copyright holder for this preprint (which was not certified by peer review) is the author/funder, who has granted bioRxiv a license to display the preprint in perpetuity. It is made available under aCC-BY-NC-ND 4.0 International license.

References

1. Gulati, G. S., D'Silva, J. P., Liu, Y., Wang, L. & Newman, A. M. Profiling cell identity and tissue architecture with single-cell and spatial transcriptomics. *Nat. Rev. Mol. Cell Biol.* 1–21 (2024).
2. Wiggins, L. *et al.* The CellPhe toolkit for cell phenotyping using time-lapse imaging and pattern recognition. *Nat. Commun.* **14**, 1854 (2023).
3. Cimini, B. A. *et al.* Optimizing the Cell Painting assay for image-based profiling. *Nat. Protoc.* **18**, 1981–2013 (2023).
4. Marchiano, S. *et al.* Gene editing to prevent ventricular arrhythmias associated with cardiomyocyte cell therapy. *Cell Stem Cell* **30**, 396-414.e9 (2023).
5. Roberts, B. *et al.* Systematic gene tagging using CRISPR/Cas9 in human stem cells to illuminate cell organization. *Mol. Biol. Cell* **28**, 2854–2874 (2017).
6. Hofbauer, P. *et al.* Cardioids reveal self-organizing principles of human cardiogenesis. *Cell* **184**, 3299-3317.e22 (2021).
7. Lewis-Israeli, Y. R. *et al.* Self-assembling human heart organoids for the modeling of cardiac development and congenital heart disease. *Nat. Commun.* **12**, 5142 (2021).
8. Park, S.-J. *et al.* Insights Into the Pathogenesis of Catecholaminergic Polymorphic Ventricular Tachycardia From Engineered Human Heart Tissue. *Circulation* **140**, 390–404 (2019).
9. Landau, S. *et al.* Primitive macrophages enable long-term vascularization of human heart-on-a-chip platforms. *Cell Stem Cell* **31**, 1222-1238.e10 (2024).
10. Sakaue-Sawano, A. *et al.* Genetically encoded tools for optical dissection of the mammalian cell cycle. *Mol. Cell* **68**, 626-640.e5 (2017).
11. Amezquita, R. A. *et al.* Orchestrating single-cell analysis with Bioconductor. *Nat. Methods* **17**, 137–145 (2020).
12. Seal, S. *et al.* From pixels to phenotypes: Integrating image-based profiling with cell health data as BioMorph features improves interpretability. *Mol. Biol. Cell* **35**, mr2 (2024).
13. Sheehy, S. P. *et al.* Quality metrics for stem cell-derived cardiac myocytes. *Stem Cell Reports* **2**, 282–294 (2014).
14. Pasqualini, F. S., Sheehy, S. P., Agarwal, A., Aratyn-Schaus, Y. & Parker, K. K. Structural phenotyping of stem cell-derived cardiomyocytes. *Stem Cell Reports* **4**, 340–347 (2015).
15. Wang, M., Da, Y. & Tian, Y. Fluorescent proteins and genetically encoded biosensors. *Chem. Soc. Rev.* **52**, 1189–1214 (2023).
16. Koh, S.-B. *et al.* A quantitative FastFUCCI assay defines cell cycle dynamics at a single-cell level. *J. Cell Sci.* **130**, 512–520 (2017).
17. Riedl, J. *et al.* Lifeact: a versatile marker to visualize F-actin. *Nat. Methods* **5**, 605–607 (2008).
18. Ohta, Y. *et al.* Cell-matrix interface regulates dormancy in human colon cancer stem cells. *Nature* **608**, 784–794 (2022).
19. Matković, J. *et al.* Kinetochore- and chromosome-driven transition of microtubules into bundles promotes spindle assembly. *Nat. Commun.* **13**, 7307 (2022).
20. Salmenov, R., Mummery, C. & Ter Huurne, M. Cell cycle visualization tools to study cardiomyocyte proliferation in real-time. *Open Biol.* **14**, 240167 (2024).
21. Caporizzo, M. A. & Prosser, B. L. The microtubule cytoskeleton in cardiac mechanics and heart failure. *Nat. Rev. Cardiol.* **19**, 364–378 (2022).
22. Kitani, T. *et al.* Human-induced pluripotent stem cell model of trastuzumab-induced cardiac dysfunction in patients with breast cancer. *Circulation* **139**, 2451–2465 (2019).
23. Burridge, P. W. *et al.* Human induced pluripotent stem cell-derived cardiomyocytes recapitulate the predilection of breast cancer patients to doxorubicin-induced cardiotoxicity. *Nat. Med.* **22**, 547–556 (2016).
24. Joshi, A. M. *et al.* Microtubule inhibitors and cardiotoxicity. *Curr. Oncol. Rep.* **23**, 30 (2021).
25. Parks, C., Alam, M. A., Sullivan, R. & Mancarella, S. STIM1-dependent Ca(2+) microdomains are required for myofilament remodeling and signaling in the heart. *Sci. Rep.* **6**, 25372 (2016).
26. Eulalio, A. *et al.* Functional screening identifies miRNAs inducing cardiac regeneration. *Nature* **492**, 376–381 (2012).
27. Bassat, E. *et al.* The extracellular matrix protein agrin promotes heart regeneration in mice. *Nature* **547**, 179–184 (2017).
28. Aratyn-Schaus, Y. *et al.* Coupling primary and stem cell-derived cardiomyocytes in an in vitro model of cardiac cell therapy. *J. Cell Biol.* **212**, 389–397 (2016).
29. Bertero, A. *et al.* Optimized inducible shRNA and CRISPR/Cas9 platforms for in vitro studies of human development using hPSCs. *Development* **143**, 4405–4418 (2016).
30. Alvarez, R., Jr *et al.* Cardiomyocyte cell cycle dynamics and proliferation revealed through cardiac-specific transgenesis of fluorescent ubiquitinated cell cycle indicator (FUCCI). *J. Mol. Cell. Cardiol.* **127**, 154–164 (2019).

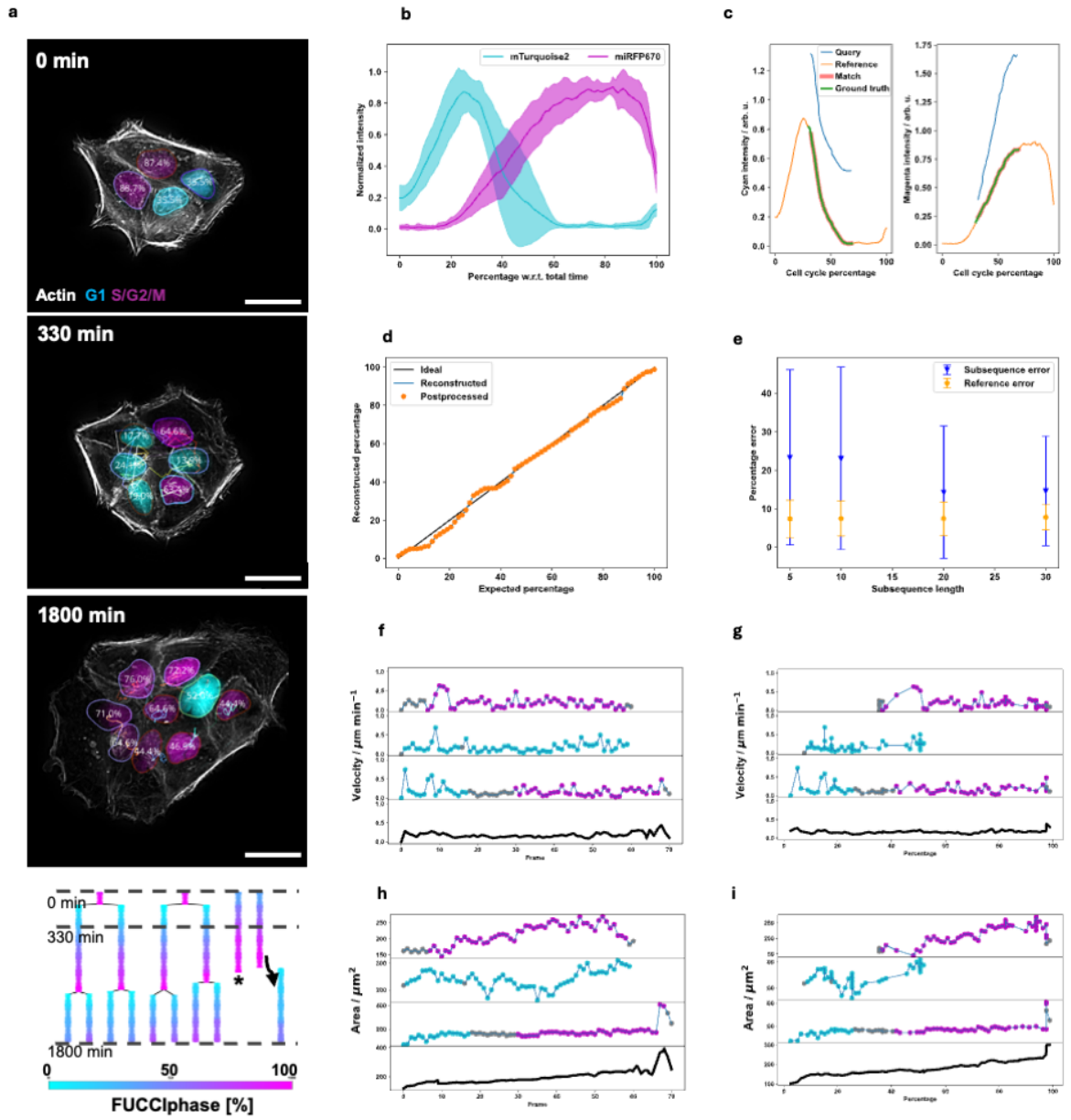
bioRxiv preprint doi: https://doi.org/10.1101/2024.12.19.629259; this version posted December 22, 2024. The copyright holder for this preprint (which was not certified by peer review) is the author/funder, who has granted bioRxiv a license to display the preprint in perpetuity. It is made available under aCC-BY-NC-ND 4.0 International license.

Extended Figures



Extended Figure 1: Deploying FUCCIplex in HaCaT cells. **a)** Live imaging of eight different clusters of HaCaT cells expressing FUCCIplex (cyan/magenta) and RFP-LifeAct (grey) **b)** Time laps- live cell imaging acquisition of HaCaT cells expressing FUCCIplex and RFP-LifeAct, followed for 18 hours. **c)** Cell cycle analysis by flow cytometry based on FUCCIplex fluorescence. **d)** Cell cycle profiles obtained by flow cytometry (propidium iodide staining). Data in this panel is also shown in abbreviated form in the manuscript's Figure 1. Details on the gating strategy are in Supplemental Figure 1. Scale bars: 50 um (a) and 100 um (b).

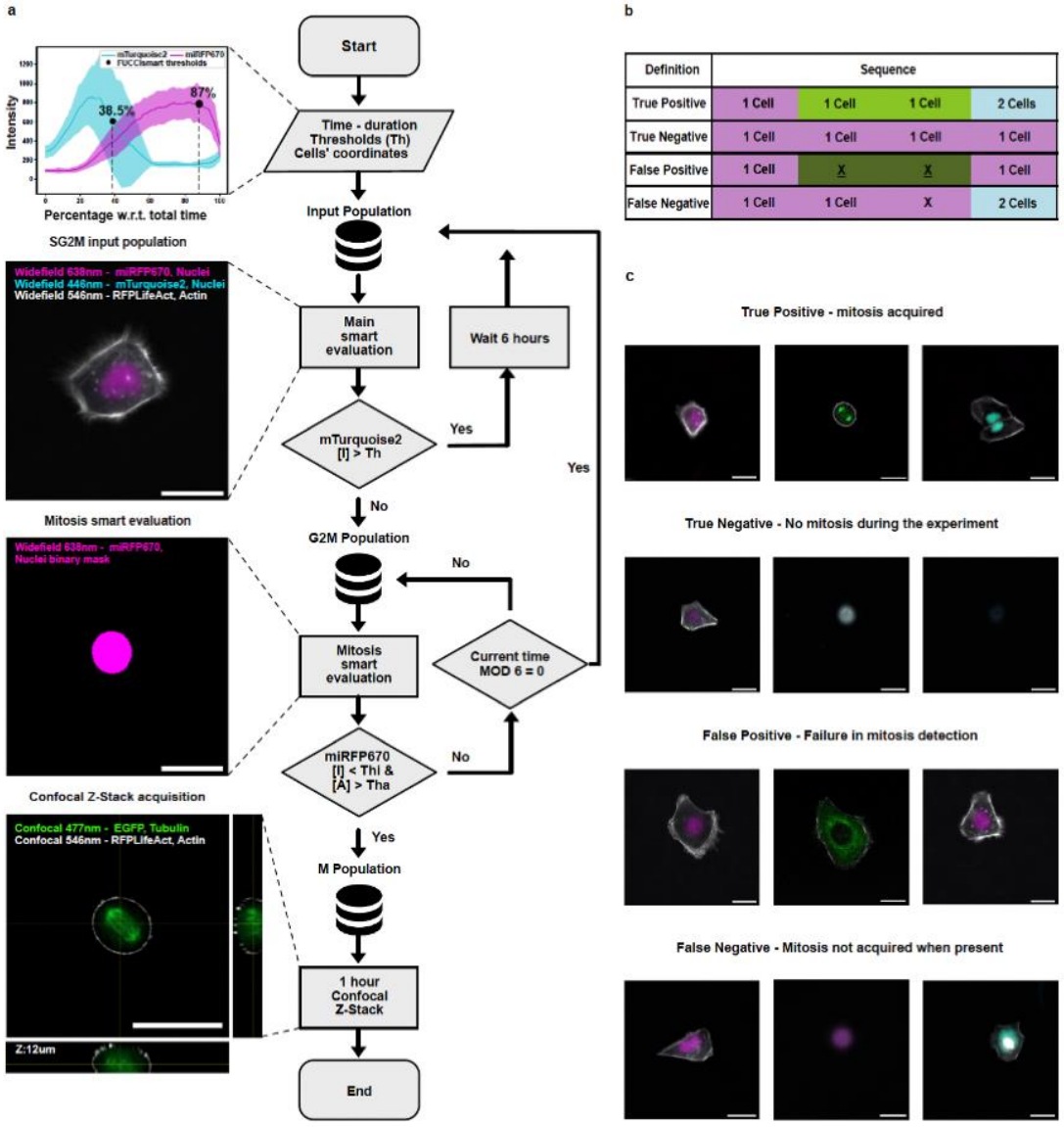
bioRxiv preprint doi: https://doi.org/10.1101/2024.12.19.629259; this version posted December 22, 2024. The copyright holder for this preprint (which was not certified by peer review) is the author/funder, who has granted bioRxiv a license to display the preprint in perpetuity. It is made available under aCC-BY-NC-ND 4.0 International license.



Extended Figure 2: **The FUCCIphase algorithm and phase-locking motility analysis. a)** Tracked nuclei with a cell cycle percentage estimate at each time point determined by the FUCCIphase algorithm. A frame from this analysis is also shown in the manuscript's Figure 1. **b)** The reference curve for HaCaT cells is distilled from 11 tracks covering the entire cell cycle. **c)** An example of sub-sequence matching was used to query cell cycle percentage from the reference curve (panel b) based on the current intensity profiles. The matched subsequence is also shown versus the ground truth subsequence. **d)** Comparison of the reconstructed versus the expected percentage (ground truth) over a full cell cycle and indicating a postprocessing step to obtain percentages with nonnegative time derivatives. **e)** Mean percentage error per sequence depending on subsequence length: thirty subsequences were sampled, and results are shown as means and standard deviation. The reference error is the error of the subsequence when the entire cycle was used (as in d). **f)** Centroid velocity as a function of the elapsed time in frames. **g)** Centroid velocity as a function of the estimated cell cycle percentage. **h)** Nucleus as a function of the elapsed time in frames. **i)** Nucleus area as a function of the estimated cell cycle percentage. **j)** Lineage tree colored according to estimated cell cycle percentage. Scale bar: 25 um (a).

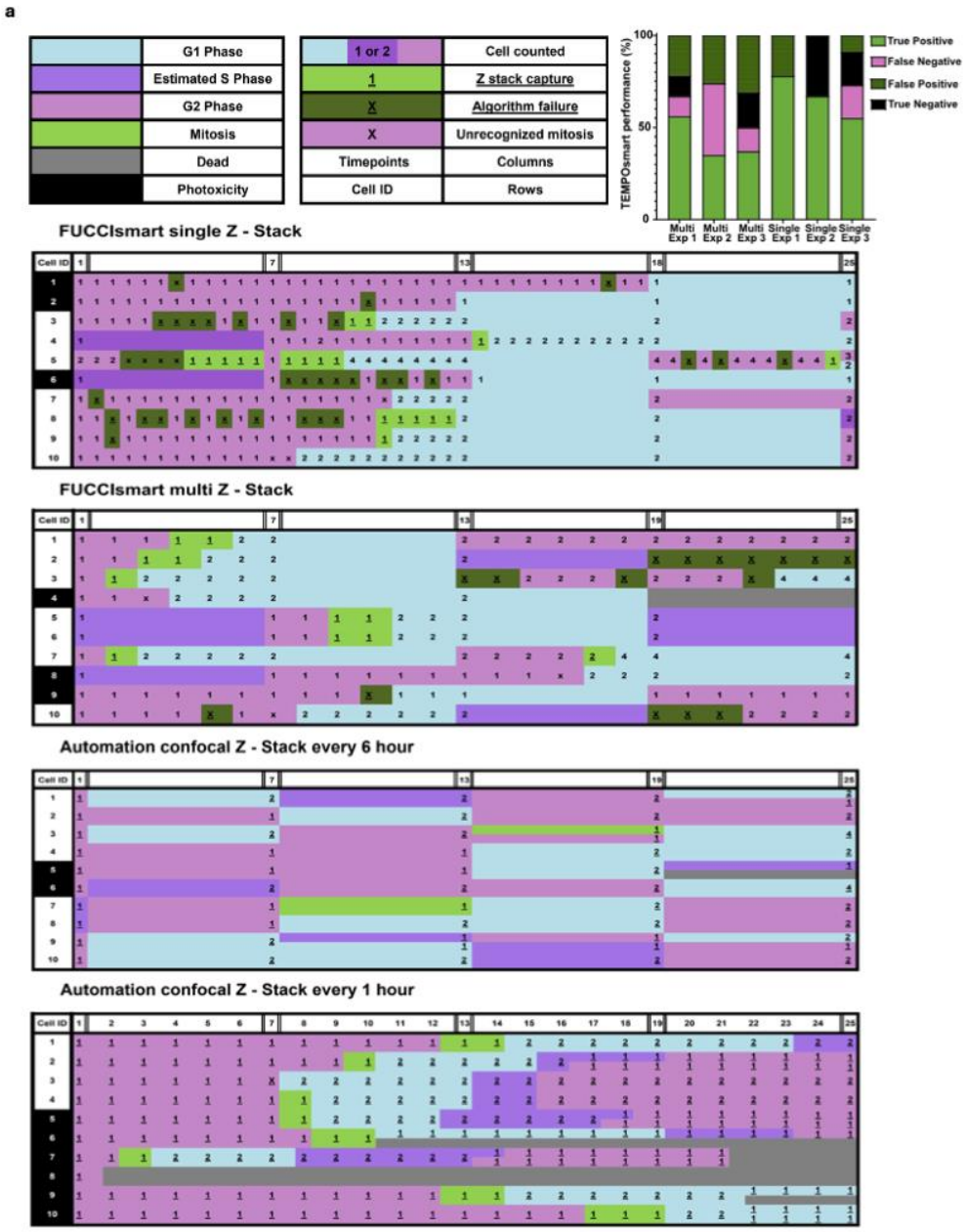
bioRxiv preprint doi: https://doi.org/10.1101/2024.12.19.629259; this version posted December 22, 2024. The copyright holder for this preprint (which was not certified by peer review) is the author/funder, who has granted bioRxiv a license to display the preprint in perpetuity. It is made available under aCC-BY-NC-ND 4.0 International license.

Extended Data Figure 3: FU



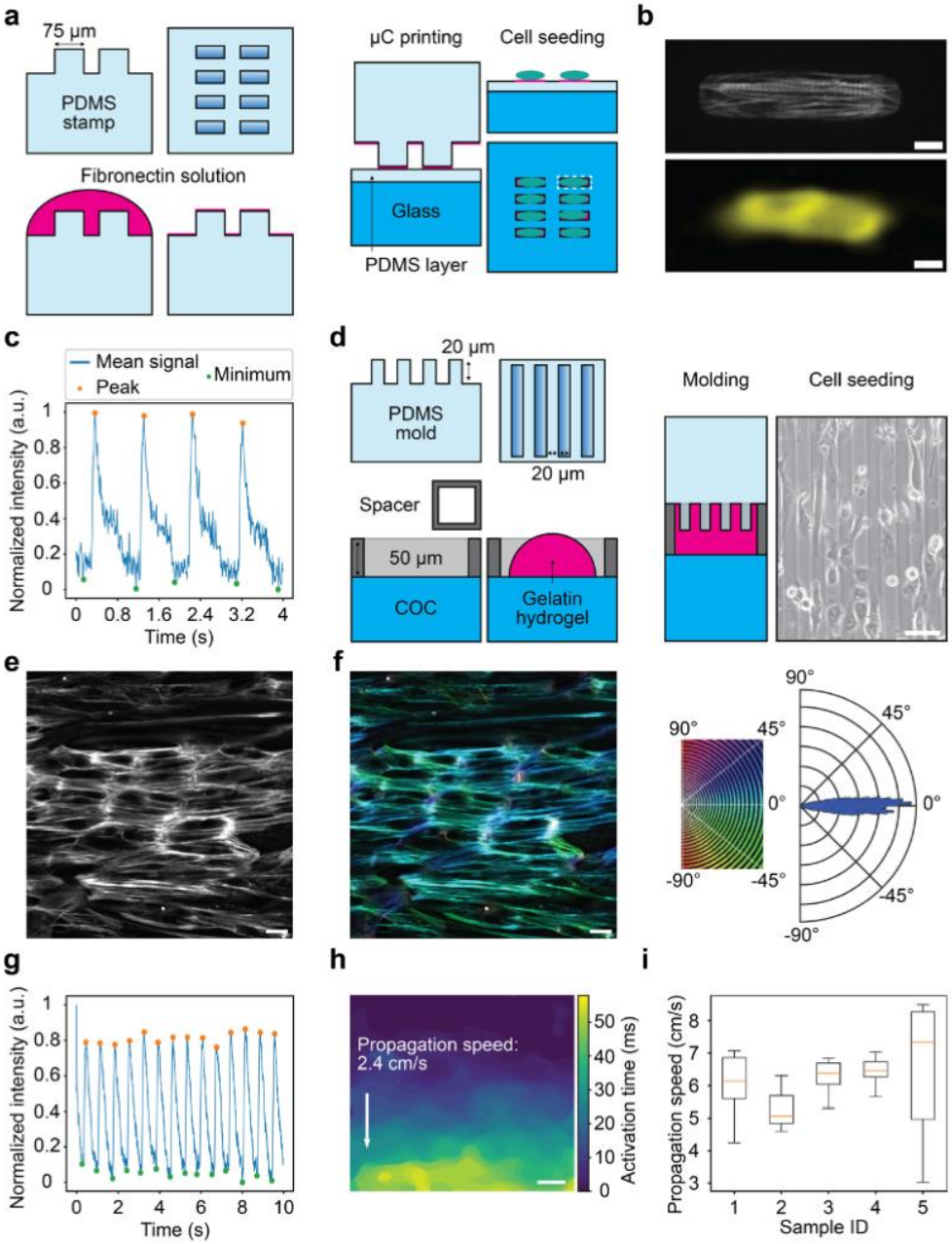
Extended Figure 3: Development and validation of FUCCIsmart. a) Flowchart illustrating our FUCCIplex-based smart microscopy (FUCCIsmart) routine as implemented in NIS Elements JOBs Module. **b)** Table summarizing FUCCIsmart classification method within the color-coded cell cycle phase sequence. **c)** Representative live imaging example of FUCCIsmart classifications within HaCaT cells with GFP-tagged β-tubulin, RFP-tagged actin, and FUCCI nuclei sensor. Scale bar: 25 µm.

bioRxiv preprint doi: https://doi.org/10.1101/2024.12.19.629259; this version posted December 22, 2024. The copyright holder for this preprint (which was not certified by peer review) is the author/funder, who has granted bioRxiv a license to display the preprint in perpetuity. It is made available under aCC-BY-NC-ND 4.0 International license.



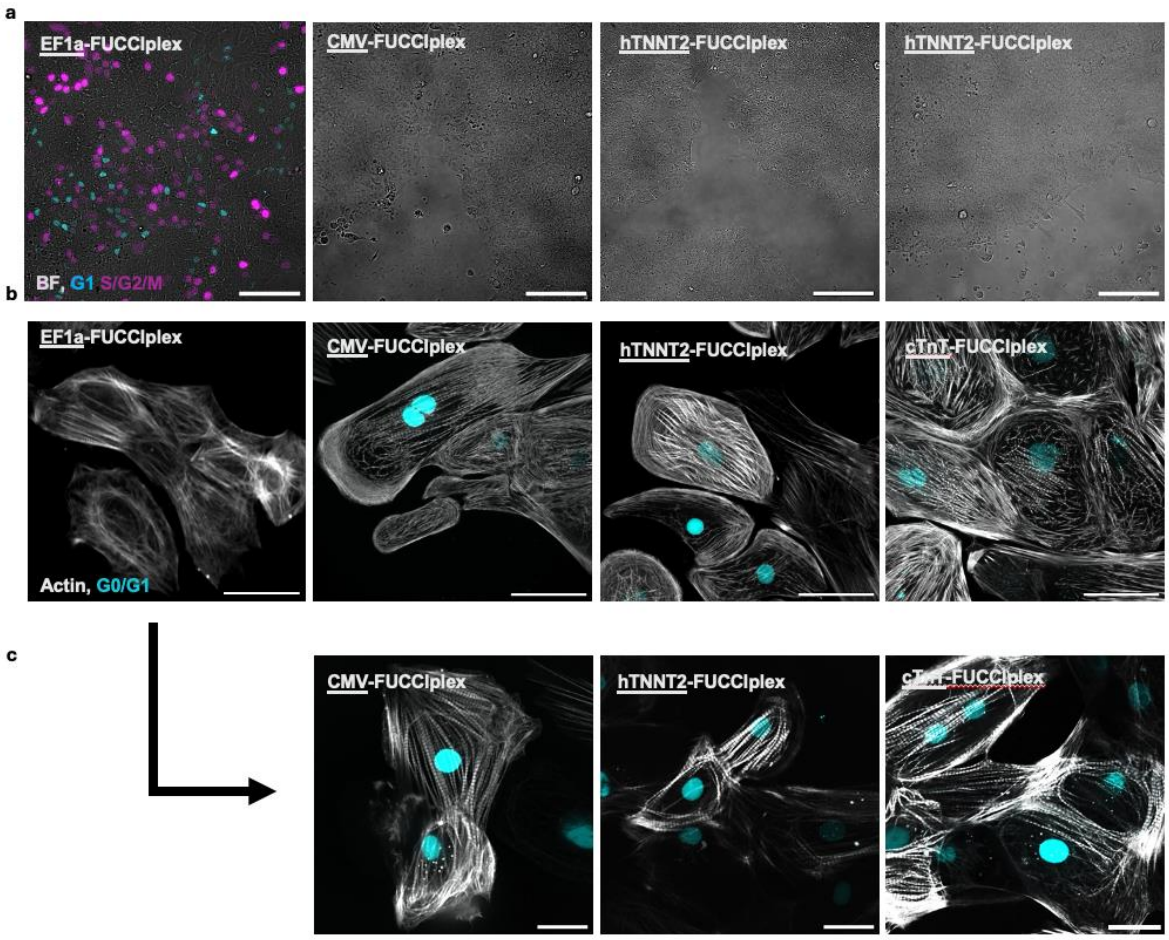
Extended Figure 4: FUCCIsmart performance evaluation tables. a) Data acquisition sequences in FUCCIsmart routines compared to confocal Automation every 6 hours and 1 hour. Rows represent individual cell recordings over 24 hours; columns correspond to the acquisition time points. Cell cycle phases are color-coded according to FUCCIplex labeling. FUCCIsmart performance was evaluated across three independent experiments. The bar graph displays True Positive, False Positive, True Negative, and False Negative percentages for both routines.

bioRxiv preprint doi: https://doi.org/10.1101/2024.12.19.629259; this version posted December 22, 2024. The copyright holder for this preprint (which was not certified by peer review) is the author/funder, who has granted bioRxiv a license to display the preprint in perpetuity. It is made available under aCC-BY-NC-ND 4.0 International license.



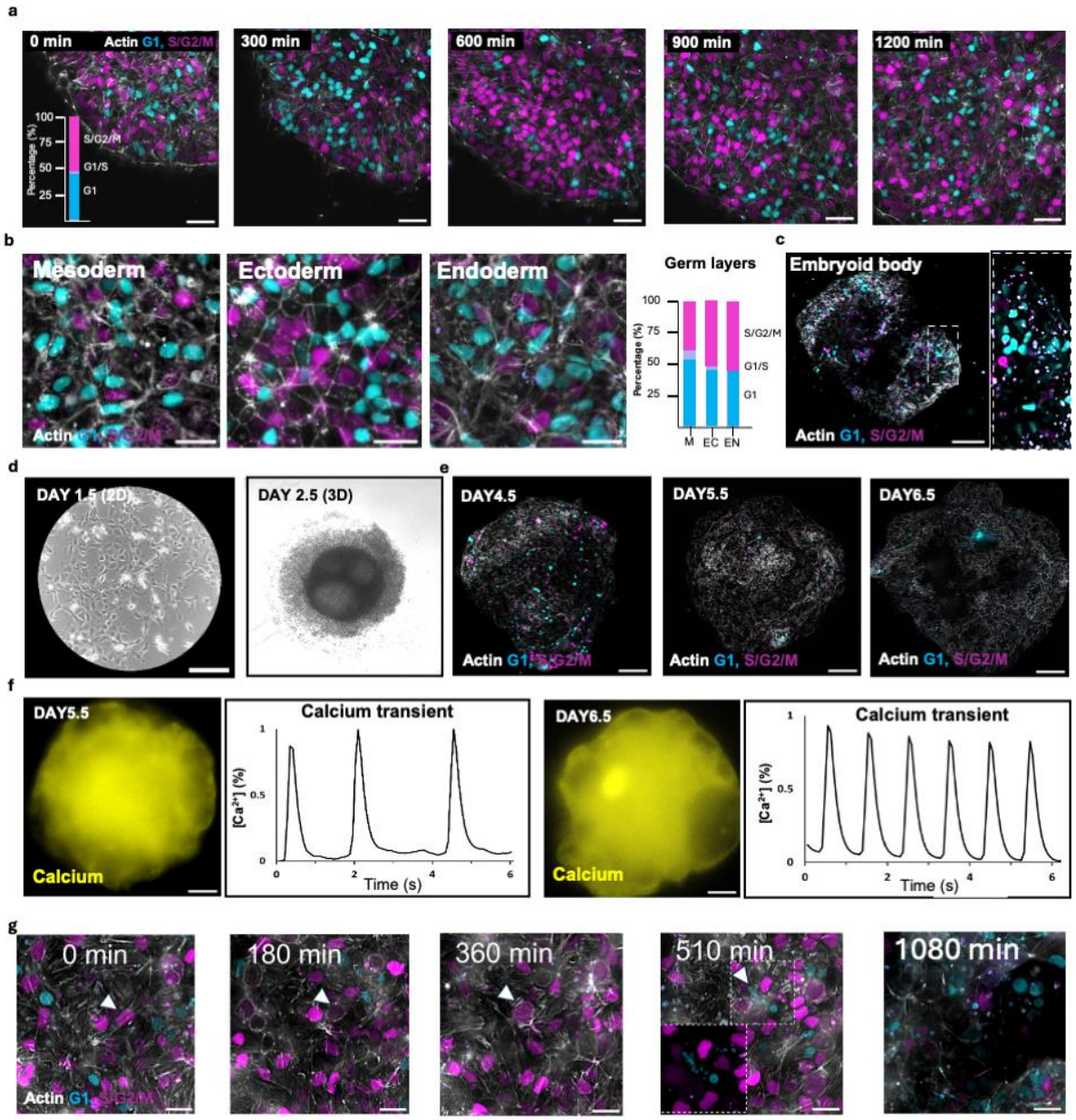
Extended Figure 5: hiPS-derived cardiomyocytes on engineered substrate. a) Schematic illustration of the microcontact printing process to ink PDMS stamps featuring cell-guiding cues and transfer the resulting fibronectin islands onto glass substrates. **b)** A confocal fluorescent image of hiPSC-CMs six days after seeding shows the calcium (yellow) and F-actin (grey) signals. **c)** Representative dynamic of calcium transient signal obtained at 25 fps recording. **d)** Schematic illustration of the micro molding process to obtain gelatin hydrogels with molded line arrays for CM tissue alignment and brightfield image of hiPSC-CMs seeded on the molded gelatin gels. **e)** Confocal fluorescent image of F-actin signal. **f)** Actin alignment analysis using OrientationJ ImageJ plugin, with colormap and radar plot showing cell alignment along the molded lines. **g)** Synchronous calcium transients in aligned hiPSC-CMs obtained at 500 fps. **h)** A representative chronomap displaying the activation time for the calcium transient obtained in g. **i)** Estimation of the average propagation speed of the calcium signal in the transversal direction with respect to the tissue alignment. Scale bars: 10 µm (b), 50 µm (d), 20 µm (e, f) and 200 µm (h).

bioRxiv preprint doi: https://doi.org/10.1101/2024.12.19.629259; this version posted December 22, 2024. The copyright holder for this preprint (which was not certified by peer review) is the author/funder, who has granted bioRxiv a license to display the preprint in perpetuity. It is made available under aCC-BY-NC-ND 4.0 International license.



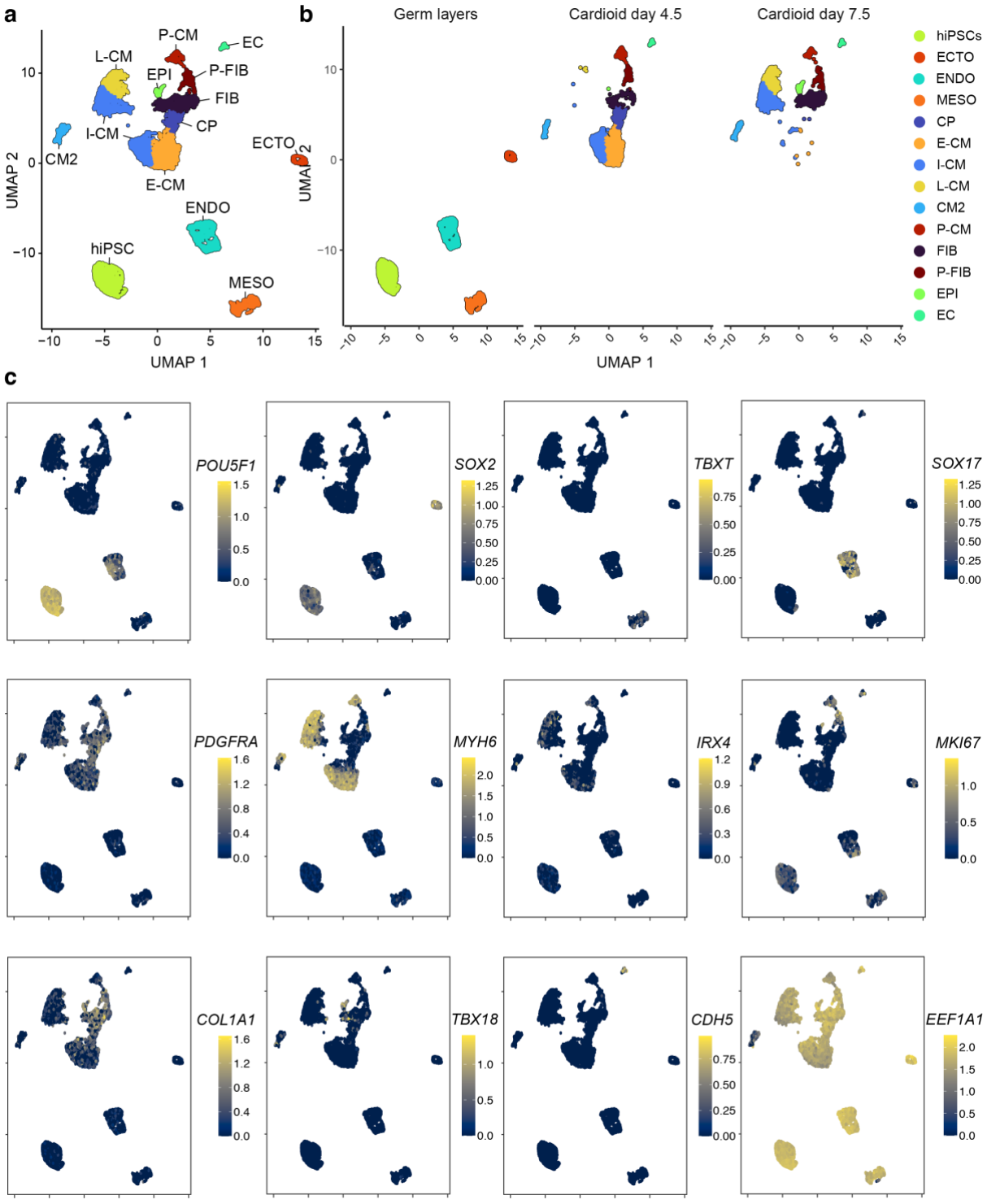
Extended Figure 6: Lentiviral transduction of different FUCCIplex constructs in hiPSC-CMs. a) Expression of FUCCIplex in hiPSCs engineered to express the calcium and actin sensor (Extended Figure 5) under the control of constitutive (EF1α and CMV) and cardiac-specific (hTNNT2 and cTnT) promoters **b)** Expression of FUCCIplex in hiPSC-CMs engineered to express the calcium and actin sensor (Extended Figure 5) under the control of constitutive (EF1a and CMV) and cardiac-specific (hTNNT2 and cTnT) promoters. **c)** Re-expression of the same viral vectors in cardiomyocytes differentiated from EF1α -FUCCIplex hiPSCs. hiPSC-CMs don't express FUCCIplex from the EF1α promoter but can express it from the CMV promoter or from cardiac-specific ones. Scale bars: 50 µm and 25 µm (b).

bioRxiv preprint doi: https://doi.org/10.1101/2024.12.19.629259; this version posted December 22, 2024. The copyright holder for this preprint (which was not certified by peer review) is the author/funder, who has granted bioRxiv a license to display the preprint in perpetuity. It is made available under aCC-BY-NC-ND 4.0 International license.



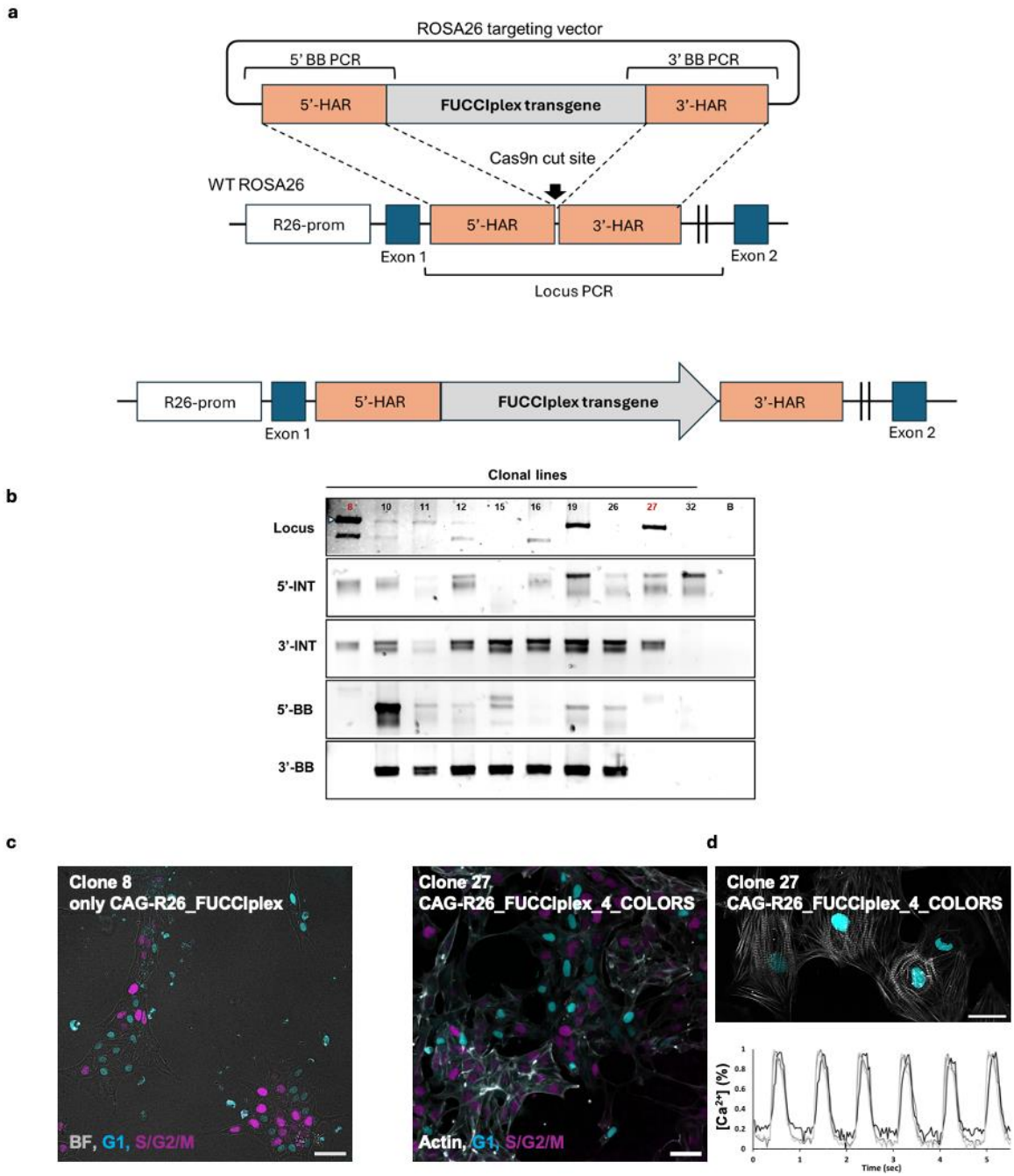
Extended Figure 7: FUCCIplex expression in hiPSCs, germ layers, embryoid bodies, and cardiac organoids. **a)** A 20-hr, time-lapse live cell imaging acquisition of hiPSCs expressing FUCCIplex (cyan/magenta) and RFP-LifeAct (grey) with quantification of how many cells are in each phase of the cell cycle (inset). **b)** Live imaging of the three germ layers derived from the hiPSC clones and cell cycle distribution. **c)** Expression of FUCCIplex and RFP-LifeAct in embryoid bodies generated from hiPSCs (day 14). **d-e)** Generation of cardiac organoids derived from hiPSCs with the passage from 2D to 3D at day 2.5. Expression of FUCCIplex, GCaMP6f, and RFP-LifeAct (grey) at days 4.5, 5.5, and 6.5. Representative calcium transients are reported only for beating organoids (days 5.5 and 6.5). **e)** Live imaging acquisition of ectoderm cells treated with Nocodazole (100 mM) and imaged every 30 minutes for 18h. An extract of data from this figure is also shown in the manuscript's figure 2. Scale bars: 50 µm (a), 25 µm (b), 100 µm (c-e), 150 µm (d), and 25 µm (f).

bioRxiv preprint doi: https://doi.org/10.1101/2024.12.19.629259; this version posted December 22, 2024. The copyright holder for this preprint (which was not certified by peer review) is the author/funder, who has granted bioRxiv a license to display the preprint in perpetuity. It is made available under aCC-BY-NC-ND 4.0 International license.



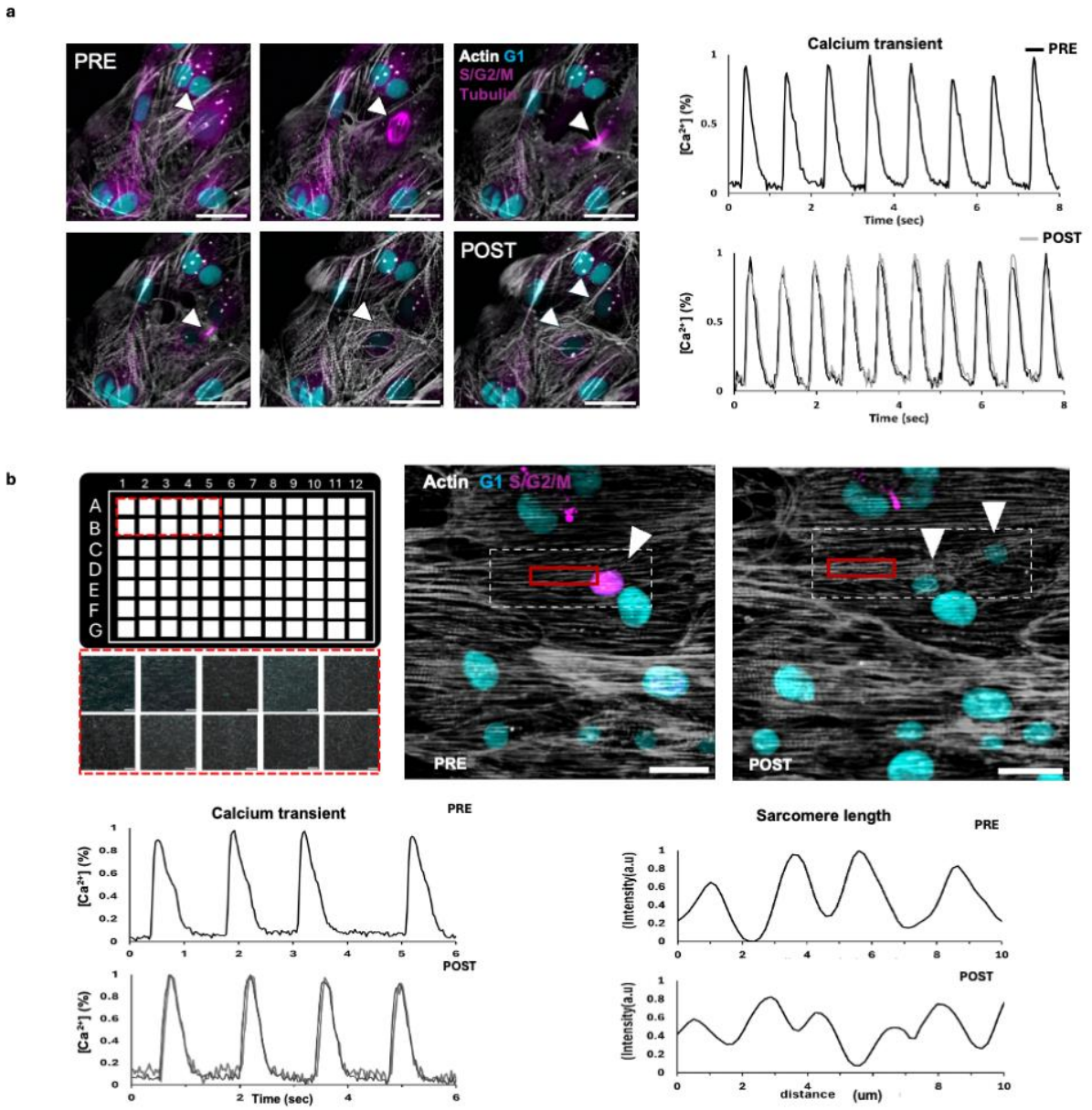
Extended Figure 8: Single-cell RNAseq analysis of human cardioids. a) Dimensionality reduction and clustering showing the main cell states and associated cell types as fingerprinted across hiPSC, germ layers, and cardioids after 4.5 and 7.5 days of differentiation. **b)** An alternative UMAP representation with a breakdown of the cell states and associated cell types in the three experimental groups. The identified cell types are hiPSCs, mesoderm, ectoderm, endoderm, and neuroectoderm; cardioid-derived cells, including cardiac progenitors, epicardial and endothelial cells, proliferating fibroblasts and cardiac fibroblasts; as well as progressively more mature hiPSC-CMs, including proliferating, early, immature, late, and conductive mature cardiomyocytes. **c)** Individual plots showing the relative expression of lineage-defining genes in the cell types represented in a-b.

bioRxiv preprint doi: https://doi.org/10.1101/2024.12.19.629259; this version posted December 22, 2024. The copyright holder for this preprint (which was not certified by peer review) is the author/funder, who has granted bioRxiv a license to display the preprint in perpetuity. It is made available under aCC-BY-NC-ND 4.0 International license.



Extended Figure 9: Genomic insertion of FUCCIplex in the ROSA26 locus and PCR screening for the detection of gene-targeted hPSC clonal lines a) Schematic diagram of the genomic insertion of the FUCCIplex construct in the ROSA26 locus. The ROSA26 targeting vector bears the FUCCIplex transgene flanked by the right left and right ROSA26 homology arms (HA). Upon homology recombination, the genome-edited cells gain a Blasticidin resistance (BSD) and the FUCCIplex transgene under the control of a CAG promoter. **b)** PCR shows the wild-type locus, the correct 5' and 3' integration (INT) of the FUCCIplex construct, the 5' and 3' off-target backbone integration (BB), and blank (B). Clone 8 (hiPSC edited only with FUCCIplex, dual color) and clone 27 (FUCCIplex positive, GCaMP6f and LifeAct-RFP, four colors) are heterozygous and no BB insertion was detected. **c-d)** Expression of ROSA26_CAG_FUCCIplex in clone 8 (only FUCCIplex) and clone 27 (four colors) hiPSC and hiPSC-CMs. BF: bright-field. Calcium traces of three different cardiomyocytes derived from clone 27. Scale bars: 50 µm (c) and 25 µm (d).

bioRxiv preprint doi: https://doi.org/10.1101/2024.12.19.629259; this version posted December 22, 2024. The copyright holder for this preprint (which was not certified by peer review) is the author/funder, who has granted bioRxiv a license to display the preprint in perpetuity. It is made available under aCC-BY-NC-ND 4.0 International license.



Extended Figure 10: Increasing content and throughput with FUCCIplex hiPSC-CMs. a) Four-color FUCCIplex hiPSC-CMs were imaged after loading with a SPY650-tubulin probe. Since M-phase miRFP670 intensity is dim in dividing hiPSC-CMs, we can clearly distinguish mitotic spindle dynamics in the nuclei (arrowhead). Calcium transients were recorded before (PRE) and after (POST) cell division. **b)** Four-color FUCCIplex hiPSC-CMs plated in a 96-well plate with a biomimetic surface (nanoSurface topography). After cardiomyocyte alignment, calcium transients and sarcomere length were quantified before (PRE) and after (POST) cell division. The dashed square and arrowheads indicate a cell before and after division. Scale bars: 25 µm (a, b).